The Journal of Experimental Biology 213, 2967-2975

doi:10.1242/jeb.041962

Comparative jet wake structure and swimming performance of salps

Kelly R. Sutherland* and Laurence P. Madin

Woods Hole Oceanographic Institution, Woods Hole, MA 02543, USA

*Author for correspondence at present address: Bioengineering, California Institute of Technology, Pasadena, CA 91125, USA (krsuth@caltech.edu)

Accepted 20 May 2010

SUMMARY

Salps are barrel-shaped marine invertebrates that swim by jet propulsion. Morphological variations among species and life-cycle stages are accompanied by differences in swimming mode. The goal of this investigation was to compare propulsive jet wakes and swimming performance variables among morphologically distinct salp species (*Pegea confoederata*, *Weelia (Salpa) cylindrica*, *Cyclosalpa* sp.) and relate swimming patterns to ecological function. Using a combination of *in situ* dye visualization and particle image velocimetry (PIV) measurements, we describe properties of the jet wake and swimming performance variables including thrust, drag and propulsive efficiency. Locomotion by all species investigated was achieved *via* vortex ring propulsion. The slow-swimming *P. confoederata* produced the highest weight-specific thrust (T=53 N kg^{-1}) and swam with the highest whole-cycle propulsive efficiency (η_{wc}=55%). The fast-swimming *W. cylindrica* had the most streamlined body shape but produced an intermediate weight-specific thrust (T=30 N kg^{-1}) and swam with an intermediate whole-cycle propulsive efficiency (η_{wc}=52%). Weak swimming performance variables in the slow-swimming *C. affinis*, including the lowest weight-specific thrust (T=25 N kg^{-1}) and lowest whole-cycle propulsive efficiency (η_{wc}=47%), may be compensated by low energetic requirements. Swimming performance variables are considered in the context of ecological roles and evolutionary relationships.

Supplementary material available online at http://jeb.biologists.org/cgi/content/full/213/17/2967/DC1

Key words: jet wakes, swimming, pelagic tunicate, propulsive efficiency.

INTRODUCTION

Salps are pelagic tunicates that swim by jet propulsion. A propulsive jet for locomotion is created by rhythmic compression of muscle bands encircling the barrel-shaped body. Fluid enters the anterior oral siphon to fill the mostly hollow body of the salp. Next, the oral lips close and circular muscle bands contract, decreasing the volume of the jet chamber so that fluid is accelerated out of the posterior, atrial siphon (Fig. 1). By the end of the jet period, the atrial siphon is closed and the oral lips open to repeat the unsteady, rhythmic process. Though swimming by jet propulsion is employed by several other marine organisms including squid, medusae and scallops, salps are unique in possessing incurrent and excurrent siphons on opposite ends of the body, allowing for unidirectional flow and reverse swimming during escape.

Among the approximately 40 species of salps, there are a range of body morphologies and swimming styles that likely relate to ecological roles of co-occurring species (Godeaux, 1998; Madin, 1990). Within each species, the salp life cycle is composed of two morphologically distinct stages; a solitary, asexually reproducing form (oozooid, Fig. 1A) buds off an aggregate, sexually reproducing form (blastozooid, Fig. 1B) comprising tens to hundreds of identical individuals. Blastozooids in turn give rise to the next generation of oozooids. Beyond the individual anatomy of blastozooids and oozooids, the arrangement of individual blastozooids into aggregate chains is also unique between species. Blastozooids are attached *via* plaques and communication between individuals allows for coordinated, though typically asynchronous, swimming and a coordinated escape response (Bone et al., 1980). Blastozooids are often asymmetrical, with atrial siphons at an angle relative to the axis of the chain. The range of body morphologies and chain architectures and associated swimming dynamics were described in detail by Madin (Madin, 1990). Fast-swimming salps are characterized by enhanced musculature, higher pulse frequencies and linear, streamlined chain structures compared with slower, surface-oriented salps.

Studies of salp swimming kinematics are few, and investigations of the jet wake properties have been limited to a single species (Bone and Trueman, 1983; Madin, 1990). The goal of this study was to compare the propulsive jet wake structure and swimming performance among different species of salps with distinct morphologies. Comparative swimming performance among salps is of particular interest because swimming and feeding are achieved by the same pumping process. In the process of drawing fluid through the body of the salp during jet propulsion, fluid and associated particles pass through a mucous filter-feeding net. Particles between 1 μm and 1 mm, primarily phytoplankton, are captured by the net and conveyed to the gut (Madin and Deibel, 1998). Therefore, a trade-off is established between these two fundamental activities.

In order to compare the kinematics and hydrodynamics of salp swimming, several species of salps representing a range of morphologies, chain architectures and swimming styles were investigated. First, the structure of propulsive jet wakes was characterized using *in situ* dye visualization and two-dimensional laboratory particle image velocimetry (PIV). Dye wake measurements provide a view of the full, 'three-dimensional' wake structure in the natural fluid environment and were used to verify that laboratory-based measurements were a reflection of normal swimming behavior. PIV is an effective technique for studying flows around aquatic organisms (Stamhuis and Videler, 1995), but this is the first application of the method to pelagic tunicate swimming. Second, kinematic and swimming performance variables were

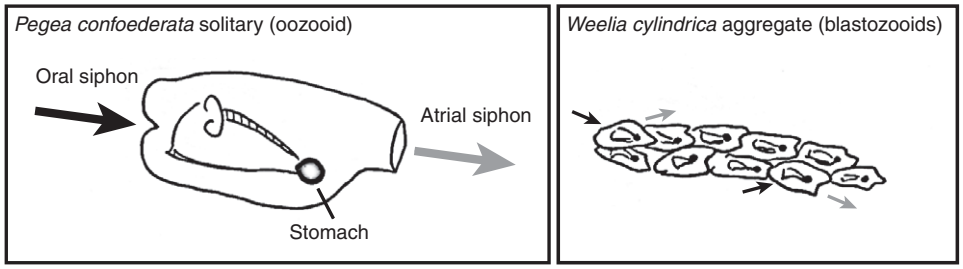

Fig. 1. Schematic illustration showing structures and fluid flow through siphons in a solitary *Pegea confoederata* and an aggregate *Weelia cylindrica*. Arrows indicate flow in through the oral siphon (black) and out through the atrial siphon (gray).

calculated from PIV video sequences. Given that swimming by salp aggregates occurs in three-dimensional space and is therefore difficult to capture with a two-dimensional tool, the PIV data and kinematic variables focus on solitary forms and the dye visualization includes both solitary and aggregate forms.

MATERIALS AND METHODS

Specimen collection and observation

Salps were collected and observed at the Liquid Jungle Lab off the Pacific Coast of Panama, Veraguas province (7°50′N, 81°35′W) during January of 2007, 2008 and 2009. The species examined represented the range of morphology and swimming kinematics among salps and included *Pegea confoederata* (Forskål 1775), *Weelia cylindrica* (Cuvier 1804), *Cyclosalpa affinis* (Chamisso 1819), *C. sewelli* (Metcalf 1927) and *C. quadriluminis* (Berner 1955). Bluewater diving techniques were used for collection and field observations (Haddock and Heine, 2005).

In situ dye visualization and laboratory PIV of salp jet wakes

Propulsive jet wakes of salps were visualized using two approaches: (1) fluorescein dye during night SCUBA dives and (2) PIV in the laboratory. SCUBA divers performed *in situ* wake flow visualizations, during night dives, using a Sony HDR-HC7 high-definition camcorder (1440×1080 pixels, 30 frames s^{-1}) with an Amphibico Dive Buddy camcorder housing and a high-intensity discharge 10 W light to illuminate the salp and dye structures. A plastic ruler placed in the field of view provided scale. Salps were approached slowly to avoid creating turbulence and fluorescein dye was ejected from a micropipette a few millimeters upstream of the oral siphon. In-focus frames that were not occluded by excess dye were selected to represent wake patterns.

Quantitative PIV data were recorded in the laboratory with salp specimens that were hand collected in 800 ml plastic jars by SCUBA divers and then maintained at field temperatures (26–28°C). Within 8 h of collection, salps were transferred from jars into custom-built acrylic tanks filled with field-collected seawater seeded with 8–12 µm titanium dioxide particles. Tanks were 6–10 l in volume depending on the size of the experimental animal. PIV allows for quantitative analysis of flow created by swimming animals in a two-dimensional plane (Adrian, 1991; Prasad, 2000; Raffel et al., 1998). The motion of small, reflective particles is measured by analyzing the positions of particles in sub-windows between successive frames. Particles were illuminated with a 300 mW, continuous green (532 nm) laser directed through a Powell lens (Lasiris/StockerYale Inc., Salem, NH, USA) to produce a 1 mm-thick light sheet. The laser was positioned to one side of the tank with the camera perpendicular to the laser sheet. In some cases, a second 300 mW laser or a mirror was placed on the opposite side of the tank to improve illumination. The motions of the particles were imaged with a Sony HDR-HC7 high-definition camcorder (1440×1080 pixels, 30 frames s^{-1}) and subsequently processed using DaVis 7.2 software (LaVision GmbH, Göttingen, Germany).

Image pairs were processed in DaVis 7.2 using a cross-correlation technique with adaptive multi-pass processing with a total of three passes (Sacrano and Riethmuller, 2000). The initial interrogation sub-window size was 128×128 pixels and the final size was 32×32 pixels with an overlap of 16 pixels. A median filter was used to remove spurious vectors. The cross-correlation processing technique maps vectors based on the spatial shift of multiple particles between successive frames in a small area (Raffel et al., 1998). Resultant velocity vector and vorticity fields were examined to identify swimming jets in which the salp and the atrial siphon remained in approximately the same lateral position for the duration of the jet. For each species, one individual jet sequence from each of four individual animals was analyzed. To enhance data visualization, background PIV image contrast was reduced and the number of vectors was doubled. Though particles >5 µm are captured by the salp filtering mesh with 100% efficiency (Kremer and Madin, 1992), the filtering mesh was typically not deployed during tank experiments. In cases where the mesh was deployed, causing low seeding in the wake, the multi-pass PIV processing technique was particularly useful because it enhances spatial resolution (Sacrano and Riethmuller, 2000).

Jet structure and velocity as well as body velocity were determined by analyzing sequences of images. Jet velocity was measured by taking a time-series of transects perpendicular to the jet, just aft of the atrial siphon, over the duration of the jetting period. Values measured just aft of the siphon were most reliable because (1) in some cases the salp was at a slight angle relative to the plane of the laser and (2) jet structures often extended beyond the field of view. Measures of whole jet wake properties such as kinetic energy, on the other hand, would be underestimates because only a portion of the jet was in the field of view. The mean jet velocity, u_m, and the maximum velocity, u_{max}, were calculated from individual transects. Since the values on either side of the jet profile approached zero, the mean jet velocity was not a good estimate of the true jet velocity. Therefore, the time average of the maximum jet velocity, u_{max}, over the entire jet period was used as the estimate of the jet velocity, $\bar{u}_j$. Because inspection of the PIV video clips revealed some streaking in the images, jet velocities were also calculated by measuring streak lengths from each image, u_s, to test the accuracy of the PIV velocity transects. Time-averaged velocities from streak measurements, $\bar{u}_s$, were not significantly different from time-averaged maximum jet velocities from PIV, $\bar{u}_j$ (*t*-test, t=–0.259, d.f.=22, P=0.8); therefore, $\bar{u}_j$ was used for time-averaged jet velocity in all calculations. Since the PIV algorithm also tracks the high-contrast portions of the salp body, body velocity was calculated by taking a series of transects through a distinguishable landmark along the body, usually the gut. The velocity values were uniform across the transect, so the mean velocities at each transect, U, were averaged to produce a time-averaged body velocity, $\bar{U}$.

Morphometric measurements of total body length, L, maximum body width, W, and maximum atrial siphon diameter, d, were obtained using ImageJ (http://rsbweb.nih.gov/ij). To adjust for size differences among salp species, swimming speed was converted to body length per time ($\overline{U}/L$). The relative streamlining of each salp species was estimated using the fineness ratio, the ratio of length to the width of a body, L/W (Vogel, 1994).

Calculation of swimming performance variables

Morphometric and kinematic data were used to calculate jet thrust, drag and propulsive efficiency. All parameters were calculated in the steady sense, using time-averaged swimming parameters. Jet thrust, T, is the rate at which an animal transfers momentum to the water and was calculated using the following equation:

$$T = \rho \overline{u}_j^2 A_j \,, \quad (1)$$

where ρ is seawater density (1021 kg m^{-3} at 28°C) and A_j is the maximum jet area determined from $\pi d^2/4$, where d is siphon diameter. Weight-specific thrust, T_w, was also determined based on relationships between live length and carbon mass (Madin et al., 1981). Drag, D, was calculated using the following equation:

$$D = \rho \overline{U}^2 A_p C_d \,, \quad (2)$$

where A_p is the projected area. For fusiform objects like salps, it is appropriate to use $A_p = V^{2/3}$, where V is body volume (Vogel, 2003). Body volumes were determined from relationships between salp length and body volume published in the literature (Madin et al., 1981; Madin and Purcell, 1992). The drag coefficient, C_d, is not constant but varies with length scale (d, siphon diameter), swimming speed (U) and kinematic viscosity ($\nu = 1.05\times10^{-6}$ m^2 s^{-1}). These quantities are incorporated into the dimensionless Reynolds number (Re) where $Re = Ud/\nu$. For $1 > Re > 500$ (Daniel, 1983):

$$C_d = 24/Re^{0.7} \,. \quad (3)$$

Slip, a measure of wasted energy, was calculated as $1 - \overline{U}/\overline{u}_j$. Propulsive efficiency was calculated in three ways: Froude propulsive efficiency, η_F, rocket motor propulsive efficiency, η_r, and whole-cycle propulsive efficiency, η_{wc} (Anderson and Demont, 2000):

$$\eta_F = 2\overline{U} / (\overline{U} + \overline{u}_j) \,, \quad (4)$$

$$\eta_r = 2\overline{U}\overline{u}_j / (\overline{U}^2 + \overline{u}_j^2) \,, \quad (5)$$

$$\eta_{wc} = 2\overline{U}\overline{u}_j / (3\overline{U}^2 + \overline{u}_j^2) \,. \quad (6)$$

Anderson and Demont (Anderson and Demont, 2000) examined the suitability of several equations of propulsive efficiency for squid swimming. Rocket motor efficiency applies during periods of fluid output only, whereas Froude propulsive efficiency applies to simultaneous fluid intake and output, as in an airscrew. Neither equation accounts for the change in momentum due to intake and deceleration of a working fluid as it enters most jet-propelled organisms. Therefore, Anderson and Demont (Anderson and Demont, 2000) derived equations both for squid whole-cycle propulsive efficiency (rear intake) and for scallop whole-cycle efficiency (forward intake) that account for losses during the refill period. The equation for scallops (Eqn 6) assumes the intake velocity to be very nearly the oncoming flow speed during refill as the valves open. This is a good assumption in salps as well, where forward motion of the body would be expected to drive fluid into the body as the lips of the oral siphon open. The whole-cycle efficiency is particularly relevant in biological systems where fluid slows as it enters the body.

RESULTS

Structure of propulsive jet wakes

In situ dye visualization showed the formation and evolution of dye wakes produced by salps swimming in the natural marine environment and PIV vector and vorticity plots provided a more quantitative view of the jet structure in two dimensions. Both methods of flow visualization showed that in all species examined, forward swimming is accomplished by vortex ring propulsion. The jet can be described as a fully pulsed jet, meaning there was a period of no flow separating pulses (Krueger and Gharib, 2003). Fluid inside the body of the salp was accelerated as circular muscle bands contracted and ejected *via* the atrial siphon. The atrial siphon was circular in cross-section at the beginning of the jet period and compressed to a horizontal slit by the end of the jet period (Fig. 2). Consecutive jets were spaced such that there was no evidence of interaction between vortex rings. Differences in the structure of the rings and trailing wakes corresponded to different swimming strategies among species and life-history stages. Jet structures ranged from discrete vortex ring 'puffs' with little or no trailing jet to a small vortex ring with a long trailing jet.

In the slow swimming *P. confoederata* solitaries (Fig. 3A, Fig. 4A,B, supplementary material Movie 1) and aggregates (Fig. 3B, supplementary material Movie 2), the majority of the ejected fluid was entrained into a vortex ring with a low-volume trailing tail. Note that though there were only two individuals in the *P. confoederata* aggregate chain in Fig. 3B, there are often tens to hundreds of individuals in a chain. The pattern of classic, circular vortex rings and no trailing jet was particularly evident in the PIV vector and vorticity plots (Fig. 4A,B).

In the fast-swimming *W. cylindrica* solitaries the jet period was short and there was a clear trailing wake with a small vortex ring, indicating that most of the ejected fluid remained in the trailing tail (Fig. 3C, Fig. 4C,D, supplementary material Movie 3). Like *W.*

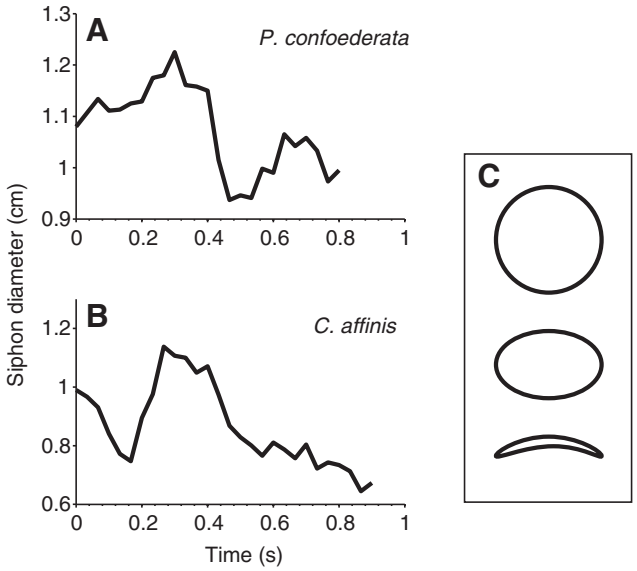

Fig. 2. Change in salp atrial siphon diameter during the jet period. (A) A 60.3 mm long *P. confoederata*, (B) 63.2 mm long *C. affinis* and (C) atrial siphon cross-section of *P. confoederata* over the course of the jet period. Drawn from an image sequence where the salp was swimming perpendicular to the 1 mm-thick laser sheet.

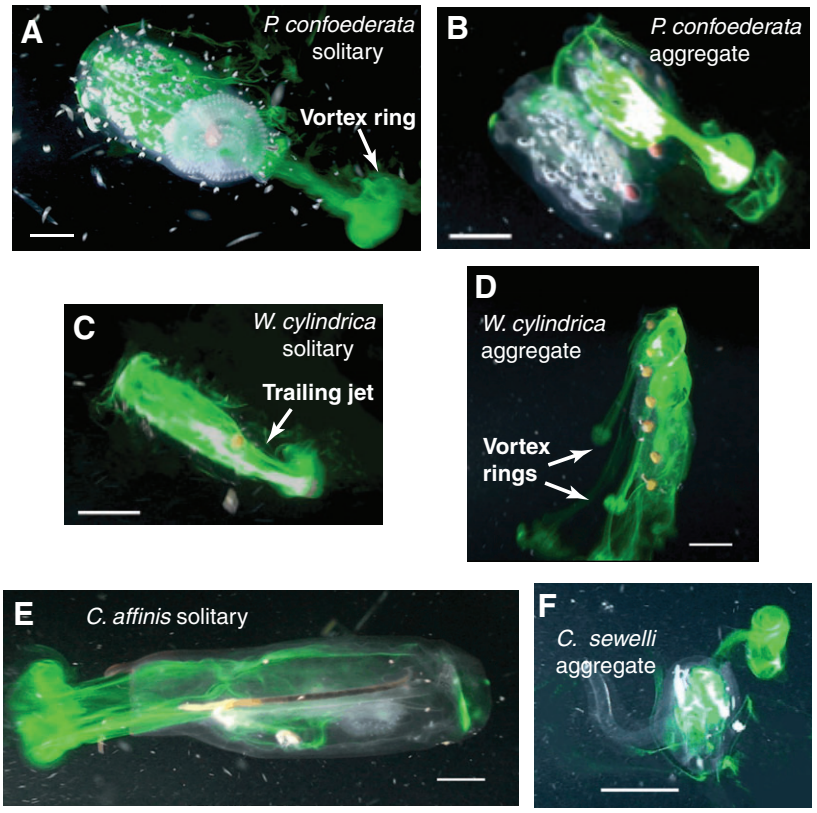

Fig. 3. *In situ* jet wake structures made visible with fluorescein dye. (A) *P. confoederata* solitary, (B) *P. confoederata* aggregate, (C) *W. cylindrica* solitary, (D) *W. cylindrica* aggregate, (E) *C. affinis* solitary and (F) *C. sewelli* aggregate. Scale bars are 1 cm.

cylindrica solitaries, *W. cylindrica* aggregates also produced a small vortex ring but the flow in the trailing tail was more elongated and appeared quite laminar (Fig. 3D, supplementary material Movie 4). Siphons are angled relative to the chain axis and therefore produced jets that propagated away from the axis of travel.

Among *Cyclosalpa* species, classic, spherical vortex rings and vortex rings with a large-volume trailing jet were observed. The solitary *C. affinis* individuals in Fig. 3E and Fig. 4E,F produced classic spherical vortex rings with little trailing jet (see also supplementary material Movie 5). In other cases, however, jet flow became unstable and turbulent (Fig. 4G,H). In *C. sewelli* aggregates, the body volume was large relative to the siphon diameter, and as the fluid was ejected almost all of it was entrained into a vortex ring with no trailing jet (Fig. 3F, supplementary material Movie 6). The individual *C. sewelli* in Fig. 3F has become detached but aggregates of this species are typically in a wheel-shape with individuals joined *via* peduncles (resembling spokes) to a central attachment point. In both *C. sewelli* and *C. quadriluminis* aggregates, which also have a wheel-like arrangement, jets were angled away from the direction of travel (Fig. 3F, Fig. 4I,J).

Kinematic swimming parameters

Salp species vary in basic morphology and swimming kinematics. Time-varying jet velocity showed distinct patterns for *P. confoederata*, *W. cylindrica* and *C. affinis* solitaries (Fig. 5). Mean jet velocity in *P. confoederata* exhibited an initial increase followed by a plateau and then a velocity peak towards the end of the jet period. In *W. cylindrica*, there was also an initial increase in jet velocity but then velocity continued to increase gradually to a maximum followed by a decline. In *C. affinis*, initial jet velocity was low and then gradually increased to a maximum followed by a relatively sharp decline. In all three species, the maximum velocity occurred about two-thirds of the way through the jet period.

Swimming kinematic data indicated that the fast-swimming *W. cylindrica* was the most streamlined, and exhibited the highest pulse frequencies and shortest jet period (Table 1). The slow-swimming *P. confoederata* was the least streamlined and had an intermediate pulse frequency and jet period length compared with the other two species. The relatively slow-swimming *C. affinis* had an intermediate degree of streamlining, the lowest pulse frequencies and the longest jet period. For salp species in general, there were no clear patterns between swimming speed (lengths s^{-1}) and jet speed or jet period (Fig. 6). Body speeds measured during the jet period were much lower than overall swimming speeds reported in the literature, suggesting that maximum body speeds occurred after the end of the jet period (Table 1). When body speed was considered in terms of specific speed (body lengths s^{-1}), *P. confoederata* and *W. cylindrica* were comparable and *C. affinis* swam slightly more slowly (Table 1).

There was no relationship between swimming speed and weight-specific thrust when all species were considered together (Fig. 7A). However, *P. confoederata* and *W. cylindrica* weight-specific thrust appeared to increase with swimming speed while that of *C. affinis* remained relatively constant. On average, *P. confoederata* exhibited substantially higher weight-specific thrust than the other two species (Table 2). Differences in drag were consistent with other swimming performance variables. The species with the lowest specific swimming speed and thrust, *C. affinis*, also experienced the highest drag (Tables 1 and 2). Slip declined and efficiency increased with increasing swimming speed (Fig. 7B,C,D), indicating that swimming at higher speeds enhances performance. As expected, Froude and rocket motor propulsive efficiencies, which do not account for energy losses during refill, were higher than whole-cycle propulsive efficiency (Table 2). Though *C. affinis* had the lowest whole-cycle propulsive efficiency, *W. cylindrica* had the lowest Froude and rocket motor efficiencies. The maximum swimming efficiency by

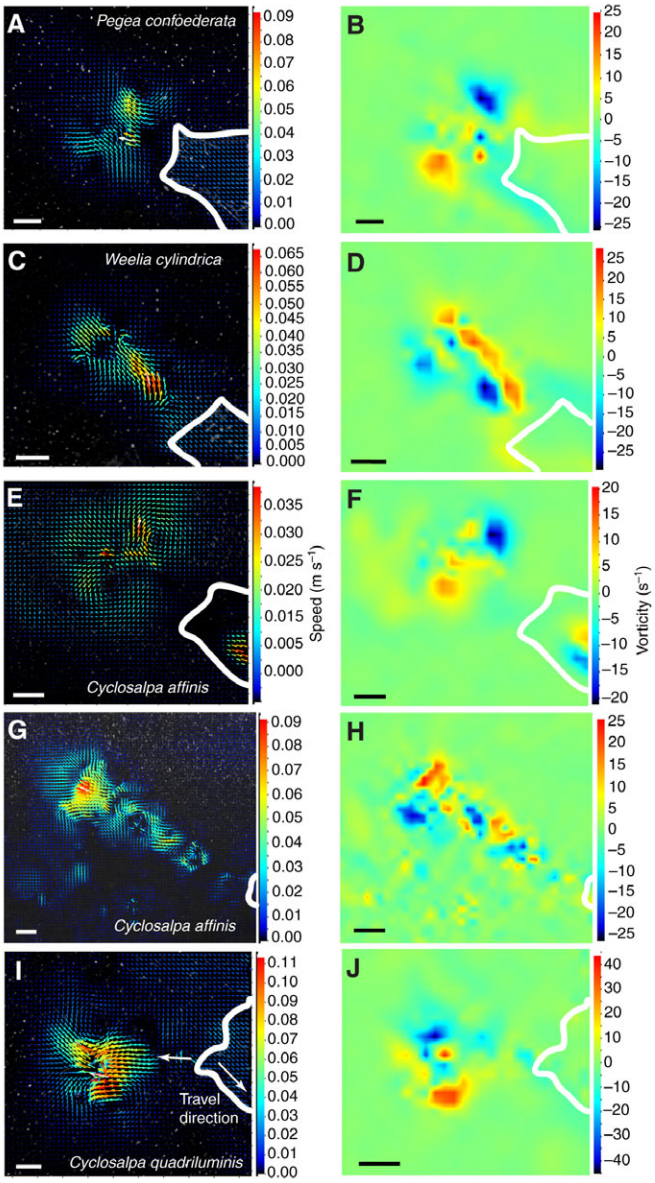

Fig. 4. Representative velocity vector (A,C,E,G,I) and vorticity (B,D,F,H,J) plots of solitary salp jet wakes with body outlines sketched in white. Scale bars are 5 mm. (A and B) Solitary *P. confoederata* with circular vortex ring, (C and D) solitary *W. cylindrica* with circular vortex ring and trailing jet, (E and F) solitary *C. affinis* with circular vortex ring, (G and H) solitary *C. affinis* with turbulent trailing jet, and (I and J) aggregate *C. quadriluminis* jet wake with circular vortex ring and slight trailing jet.

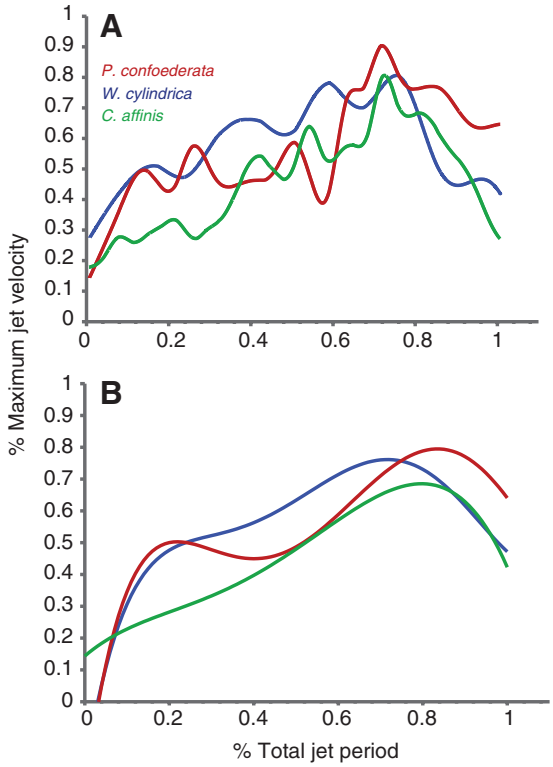

Fig. 5. (A) Mean jet velocity during jet period for *P. confoederata*, *W. cylindrica* and *C. affinis*. Each jet is normalized to the same duration and expressed as % of maximum velocity to allow for comparisons between species. *N*=4 for each species. (B) Polynomial fits to curves plotted in A.

all three propulsive efficiency measures was achieved by *P. confoederata*.

DISCUSSION

Aspects of salp jet wake structure

The findings presented here represent the first comparative study of salp jet wake structure and swimming performance. General aspects of salp jet propulsion in all species and life-history stages included: (1) fully pulsed jets, meaning there was a period of no flow between pulses, (2) production of vortex rings during each pulse (Figs 3 and 4, supplementary material Movies 1–6), and (3) an initial increase in siphon diameter followed by a decrease over the course of the jet period (Fig. 2). Based on an analytical model, Weihs (Weihs, 1977) showed that closely spaced periodic jets result in substantial increases in thrust. More recent studies with squid and a mechanical pulsed-jet vehicle have confirmed a thrust benefit from pulsing compared with a continuous jet (Krueger et al., 2008). As a vortex ring forms, ambient fluid is accelerated and entrained in the growing ring. Variation in siphon diameter can delay pinch off of the ring from a trailing jet so that even more fluid is entrained in the vortex ring (Dabiri and Gharib, 2005). Each of these features, characteristic of salp jet propulsion, were associated with the entrainment of additional, ambient fluid which leads to increased thrust (Dabiri, 2009; Krueger and Gharib, 2003; Krueger et al., 2008).

Though vortex ring propulsion was common to all species in this study, diverse morphologies and swimming kinematics were related to differences in swimming speed and performance. Propulsion was achieved in *P. confoederata* solitaries and aggregates *via* classic vortex ring puffs (Fig. 3A,B, Fig. 4A,B) whereas *W. cylindrica* solitaries and aggregates produced vortex rings with a trailing jet (Fig. 3C,D, Fig. 4C,D). Among *Cyclosalpa* species, a combination of isolated vortex rings and vortex rings with trailing wakes was observed (Fig. 3E,F, Fig. 4E–H). Each species also employed a characteristic velocity profile during jet formation that relates to swimming parameters (Fig. 5). For example, fluid acceleration by *P. confoederata* and *W. cylindrica* during jet initiation increases fluid momentum and helps explain higher weight-specific thrust in these species.

The range of wake structures observed among salps is bracketed by the two jet modes described in the squid, *Lolliguncula brevis*, throughout ontogeny (Bartol et al., 2009) and also observed among

Table 1. Morphometric and kinematic variables for solitary stage salps

	Pegea confoederata	*Weelia cylindrica*	*Cyclosalpa affinis*
Number of individuals	4	4	4
Length (mm)	50.8 (39.0–60.3)	39.5 (36.0–43.4)	64.1 (63.2–65.0)
Carbon mass (mg)[a]	1.61 (1.23–1.92)	1.63 (1.36–1.95)	4.29 (4.18–4.40)
Swimming speed (cm s^{-1})[b]	4.1 (1.7–5.6)	6.0 (2.5–13.9)	4.8 (2.5–5.9)
Re	433 (132–635)	196 (120–271)	380 (179–687)
Pulse frequency (Hz)[c]	1.5	2	0.8
Jet period (s)	0.52 (0.37–0.80)	0.36 (0.2–0.43)	0.69 (0.53–0.93)
Fineness ratio	2.12 (1.92–2.40)	2.59 (2.16–2.96)	2.26 (1.90–2.73)
Body speed (cm s^{-1})	1.68 (0.81–2.22)	1.23 (0.85–1.60)	1.72 (0.87–3.11)
Body speed (lengths s^{-1})	0.32 (0.21–0.41)	0.31 (0.22–0.41)	0.27 (0.14–0.50)
Jet speed (cm s^{-1})	3.27 (2.03–4.64)	3.34 (3.23–4.25)	3.30 (2.52–3.89)

Note that body speed was measured during jet period only. Values are means with ranges in parentheses.
Re, Reynold's number.
[a]Carbon mass calculated from relationships between length and weight (Madin et al., 1981).
[b]Data are from Madin (1990).
[c]Data are averaged from Madin (1990) and Sutherland and Madin (2010).

jellyfish species (Dabiri et al., 2010). In jet mode I, which was associated with higher propulsive efficiency, all of the fluid ejected from the siphon was entrained into an isolated vortex ring. In jet mode II, which was associated with greater thrust but lower propulsive efficiency, some of the fluid was entrained into a leading vortex ring but the remainder formed a long trailing jet. The finding that isolated vortex rings were more efficient than vortex rings with trailing jets is consistent with studies using mechanical pulsed jets (Krueger et al., 2008). Though different propulsive efficiency equations were used in the squid and jellyfish studies (Bartol et al., 2009; Dabiri et al., 2010), our calculations show that *P. confoederata*, which consistently produced isolated vortex rings (i.e. jet mode I), also had the highest Froude propulsive efficiency (Table 2). Conversely, *W. cylindrica* produced leading vortex rings with a trailing jet, and had the lowest Froude propulsive efficiency (Table 2). In contrast with squids, leading vortex rings with a trailing jet (i.e. jet mode II) observed in *W. cylindrica* and occasionally in *C. affinis* were not associated with higher thrust in salps (Table 2). In general, salp jet wake structure does not fall neatly into the two jet mode categories but rather falls along a continuum from isolated vortex ring to vortex rings with varying degrees of a trailing jet. A similar continuum of jet wake structure was observed in squids (Bartol et al., 2009).

Pulsed jets can be considered in the context of recent work on optimal vortex ring propulsion. Studies using mechanically generated jets have shown that thrust is maximized when the jet length-to-diameter ratio, called the formation number (F), lies between 3.6 and 4.5 (Gharib et al., 1998). Above this optimum range, the leading vortex ring becomes disconnected or 'pinched off' and is followed by a trailing jet. Recent work with jet-propelled organisms has revealed that the formation numbers at which discrete vortex rings are formed may differ from this optimum. Pipe jet experiments and studies with jet-propelled organisms have shown that the optimum F can be affected by at least two phenomena: (1) background co-flow can lower the optimum F due to early pinch-off or inhibition of vortex rings, leading to elongated jets with weak or absent vortex rings (Anderson and Grosenbaugh, 2005; Krueger et al., 2003) and (2) variation in jet diameter and/or jet velocity can delay pinch-off (Dabiri and Gharib, 2005). The jets of steadily swimming squid, which always experience co-flow due to flow past the squid, occur at formation numbers of F=5.5–61.8 (adult *Loligo pealei*) and F=3.23–23.19 (juvenile and adult *Lolliguncula brevis*) (Anderson and Grosenbaugh, 2005; Bartol et al., 2009). These ranges extend well above 3.6–4.5 and since co-flow reduces optimum F, squid jet events are sometimes elongated plugs of fluid rather than discrete vortex rings (Anderson and Grosenbaugh, 2005). Variation in jet diameter by *Nemiopsis bachei*, a cnidarian jellyfish species that swims by jet propulsion, led to a maximum F of around 8, and vortex ring pinch-off never occurred (Dabiri et al., 2006). Certain features of salp jet propulsion, including a variable atrial siphon diameter (Fig. 2) and fluid acceleration for the first two-thirds of the jet period (Fig. 5), may lead to vortex formation numbers greater than the optimum range. Further work, likely using three-dimensional techniques, will be needed to fully resolve aspects of vortex formation and structure among salps.

Swimming morphology, kinematics and performance

It has previously been shown that higher swimming speeds in salps are related to higher pulse frequencies (Madin, 1990). In the present study, the fastest swimming species, *W. cylindrica*, had the highest

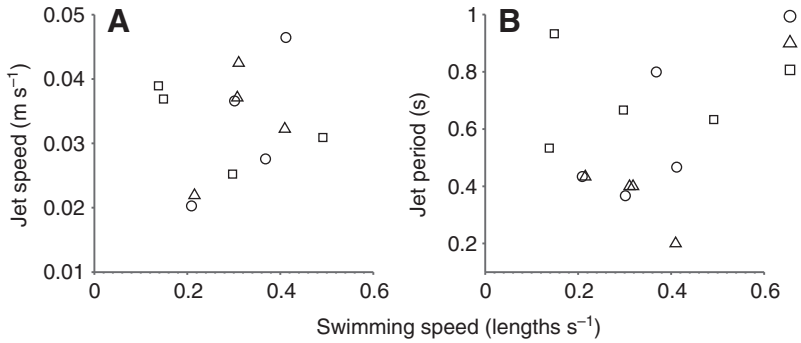

Fig. 6. (A) Jet speed and (B) jet period as a function of specific swimming speed for *P. confoederata*, *W. cylindrica* and *C. affinis*.

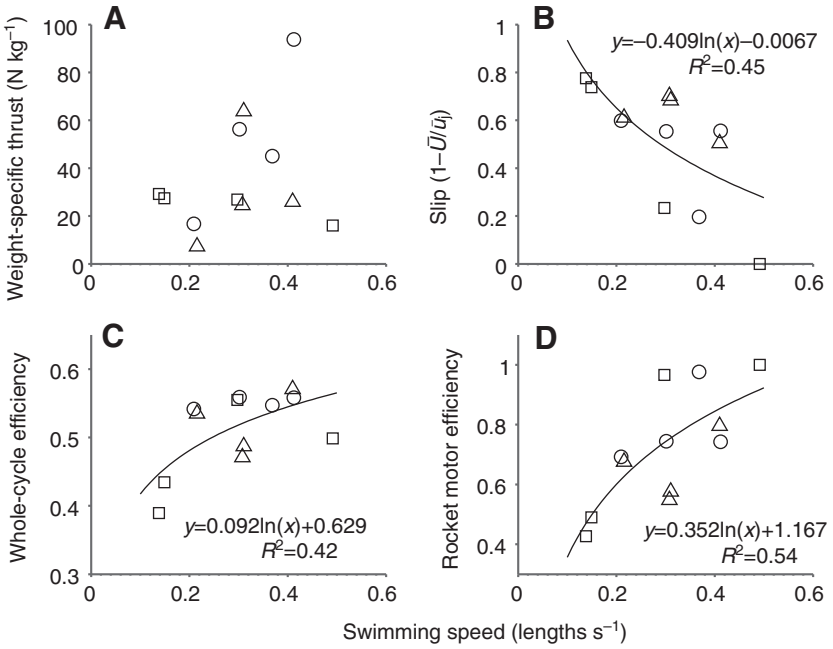

Fig. 7. (A) Weight-specific jet thrust, (B) slip (1–$\bar{U}/\bar{u}_j$), (C) whole-cycle propulsive efficiency (Anderson and Demont, 2000), and (D) rocket motor propulsive efficiency as a function of specific swimming speed for *P. confoederata*, *W. cylindrica* and *C. affinis*.

pulse frequencies, as well as the shortest jet periods, most streamlined form, lowest drag and the highest jet speeds (Tables 1 and 2). Weight-specific thrust, however, was relatively low in *W. cylindrica* owing to a small jet area relative to body size. Conversely, the slowest swimming species examined in this study, *P. confoederata*, produced the highest weight-specific thrust and swam with the greatest propulsive efficiency (Tables 1 and 2). Swimming performance variables indicated that *C. affinis* was the weakest swimmer, exhibiting the lowest weight-specific thrust, highest drag and lowest whole-cycle propulsive efficiency (Table 2). However, the variables measured in this study relate to hydrodynamic efficiency which does not consider the energetic cost of swimming. Across all species, both whole-cycle and rocket motor propulsive efficiency increased with speed with a concomitant decrease in slip (Fig. 7B,C,D). A maximum efficiency and low slip at higher speeds might be beneficial for vertically migrating salp species, which travel hundreds of meters over a 24 h cycle (e.g. Madin et al., 2006).

Swimming thrust and efficiency measurements from the current study differed from those measured in *Salpa fusiformis* (Bone and Trueman, 1983). Thrust measurements in the two studies deviated by an order of magnitude and since *S. fusiformis* is similair in size, streamlining and swimming speed to *W. cylindrica*, this was unexpected. Bone and Trueman approximated thrust two ways: using measurements of static thrust and chamber pressure, as well as using estimates of mass and maximum acceleration (Bone and Trueman, 1983). Since our measurements were based on jet velocity and jet area, it is not possible to resolve this discrepancy. However, experimental artifact due to low-volume containers, tethering and outfitting of specimens with pressure transducers and strain gauges in the Bone and Trueman study (Bone and Trueman, 1983) may partially account for the differences. Propulsive efficiency of *S. fusiformis*, calculated from maximum jet and body velocities in the study of Bone and Trueman (Bone and Trueman, 1983) were much lower than those measured in the present study, ranging from 17% to 46% though the authors reported that they would expect higher efficiencies at cruising speeds.

From the standpoint of the salp, whole-cycle propulsive efficiency is of greatest relevance for ecological performance. The equation for whole-cycle propulsive efficiency (Anderson and Demont, 2000) has a maximum theoretical efficiency of 58% and *P. confoederata* came close to achieving this upper bound, with a mean efficiency of 55% (Table 2). Nonetheless, even the species with the lowest measured mean efficiency of 47% (*C. affinis*) was still relatively efficient. However, since the filtering mesh was not typically deployed during lab PIV, efficiency may be an overestimate. The resistance of the filter would be expected to reduce volume flow rate through the salp but this effect would be uniform across species and would not change relative efficiencies. Furthermore, *in situ* wake structures, when filtering meshes were deployed, were qualitatively similar to PIV wake structures (Figs 3 and 4).

Salps in this study had higher whole-cycle propulsive efficiencies than squid. Efficiency for the squid *L. brevis* ranges from 29% to

Table 2. Swimming performance variables for solitary stage salps

	Pegea confoederata	*Weelia cylindrica*	*Cyclosalpa affinis*
Number of individuals	4	4	4
Thrust (N $\times 10^5$)	8.82 (2.05–14.89)	5.27 (1.19–12.44)	10.7 (6.69–12.23)
Weight-specific thrust (N kg^{-1})	53.0 (16.7–93.9)	30.4 (24.5–72.9)	24.9 (16.0–29.2)
Drag (N $\times 10^5$)	1.50 (1.43–5.84)	1.04 (0.70–1.41)	4.07 (1.19–8.59)
Froude propulsive efficiency	0.67 (0.61–0.89)	0.54 (0.48–0.66)	0.66 (0.37–1.00)
Rocket motor propulsive efficiency	0.78 (0.69–0.98)	0.65 (0.55–0.80)	0.72 (0.43–1.00)
Whole-cycle propulsive efficiency	0.55 (0.54–0.56)	0.52 (0.47–0.57)	0.47 (0.39–0.56)

Values are means with ranges in parentheses.

44% and efficiency for the squid *L. pealei* ranges from 34% to 48% (Bartol et al., 2001; Anderson and Demont, 2000). In comparison to squid, salps have siphons on opposite ends of the body so losses due to intake are smaller. Salps swim continuously using a high-volume, low-velocity jet, which also drives a feeding current. Squid on the other hand, do not need to swim continuously and can also rely on fin motion to aid in swimming. For squid, speed and maneuverability may be enhanced at the cost of propulsive efficiency.

Though the swimming efficiencies of blastozooid chains were not measured in this study, Bone and Trueman (Bone and Trueman, 1983) found that a chain of actively swimming *S. fusiformis* swam at even higher efficiencies than individual blastozooids or oozoids. The arrangement of individuals in chains as well as the coordination of pulses and maneuvering within chains are important aspects of salp locomotion that warrant further investigation.

Ecological and evolutionary context for swimming patterns

A comparison of swimming performance among this group of morphologically distinct organisms naturally leads to questions about the ecological function of swimming characteristics as well as evolutionary relationships. The production of isolated vortex rings, along with high weight-specific thrust and high whole-cycle propulsive efficiency of *P. confoederata* suggests that this species has evolved traits for highly economical swimming. Conversely, swimming by *C. affinis* is characterized by a trailing jet, low weight-specific thrust and whole-cycle propulsive efficiency. Intriguingly, a recent molecular phylogeny of the Thaliaceans supports *Pegea* spp. as part of an ancestral lineage, whereas the *Cyclosalpa* spp. occupy a more derived position, paraphyletic with the Salpinae (A. F. Govindarajan, A. Bucklin and L.P.M., unpublished data). Since pumping fulfills a dual role of propulsion and feeding, one might surmise that though cyclosalps are poor swimmers, perhaps they are effective filter feeders. However, this is not the case. Though there is considerable scatter in filtration rate measurements depending on the methods used, previous studies have generally shown *C. affinis* to have some of the lowest filtration rates (Madin and Deibel, 1998). The most recent work, conducted in conjunction with this study, showed that *C. affinis* had the lowest normalized filtration rates, *P. confoederta* had intermediate rates and *W. cylindrica* had the highest rates, though rates were not significantly different between species (Sutherland and Madin, 2010). It is also of interest that *W. cylindrica* is both fast swimming and has high filtration rates. Both of these traits are likely tied to the high pulse frequency in this species.

Still, a complete picture of trade-offs in swimming and feeding requires consideration of energetic requirements of different species. Weight-specific respiration rates of *C. affinis* and other *Cyclosalpa* spp. are indeed low compared with other species, suggesting a lower energetic cost of locomotion (Madin and Deibel, 1998). This is consistent with the lifestyle of Cyclosalps, which are non-migratory and possess a thin, watery tunic that probably takes relatively little energy to compress. Faster swimming and more streamlined species, including *W. cylindrica* and *Salpa* spp., have some of the highest weight-specific respiration rates (Madin and Deibel, 1998). Considering that several *Salpa* species make extensive diel vertical migrations, high swimming speeds that are also relatively hydrodynamically and energetically inefficient may be a necessary cost that is compensated for by higher filtration rates. In conjunction with recent phylogenetic and filtration rate studies, the results if this work enhance our understanding of the evolution of diverse form and function in this important holoplanktonic group.

LIST OF SYMBOLS AND ABBREVIATIONS

A_j	maximum jet area
A_p	projected area
C_d	drag coefficient
d	maximum atrial siphon diameter
D	drag
F	formation number
L	body length
PIV	particle image velocimetry
Re	Reynolds number
T	jet thrust
T_w	weight-specific thrust
U	body velocity during jet period
$\overline{U}$	time-averaged body velocity during jet period
$\bar{u}_j$	time-averaged maximum jet velocity
u_m	mean jet velocity
u_{max}	maximum jet velocity
u_s	jet velocity from streak lengths
$\bar{u}_s$	time-averaged jet velocity from streak lengths
V	body volume
v	kinematic viscosity
W	maximum body width
η_F	Froude propulsive efficiency
η_r	rocket motor propulsive efficiency
η_{wc}	whole-cycle propulsive efficiency
ρ	seawater density

ACKNOWLEDGEMENTS

We gratefully acknowledge the people who facilitated our work at the Liquid Jungle Lab including Luis Camilli and Ellen Bailey. Dan Martin, David Kushner, Andrew Gray, Emily Abbott, Alex Techet and David Sutherland helped with SCUBA work. Erik Anderson and Alex Techet provided useful suggestions in analyzing data and interpreting results. The comments of two anonymous reviewers improved the quality of the manuscript. This research was funded by the National Science Foundation (OCE-0647723) and a *Journal of Experimental Biology* traveling fellowship.

REFERENCES

Adrian, R. J. (1991). Particle-imaging techniques for experimental fluid-mechanics. *Annu. Rev. Fluid Mech.* **23**, 261-304.

Anderson, E. J. and Demont, M. E. (2000). The mechanics of locomotion in the squid *Loligo pealei*: locomotory function and unsteady hydrodynamics of the jet and intramantle pressure. *J. Exp. Biol.* **203**, 2851-2863.

Anderson, E. J. and Grosenbaugh, M. A. (2005). Jet flow in steadily swimming adult squid. *J. Exp. Biol.* **208**, 1125-1146.

Bartol, I. K., Patterson, M. R. and Mann, R. (2001). Swimming mechanics and behavior of the shallow-water brief squid *Lolliguncula brevis*. *J. Exp. Biol.* **204**, 3655-3682.

Bartol, I. K., Krueger, P. S., Stewart, W. J. and Thompson, J. T. (2009). Hydrodynamics of pulsed jetting in juvenile and adult brief squid *Lolliguncula brevis*: evidence of multiple jet `modes' and their implications for propulsive efficiency. *J. Exp. Biol.* **212**, 1889-1903.

Bone, Q. and Trueman, E. R. (1983). Jet propulsion in salps (Tunicata: Thaliacea). *J. Zool. Lond.* **201**, 481-506.

Bone, Q., Anderson, P. A. V. and Pulsford, A. (1980). The communication between individuals in salp chains. I. Morphology of the system. *Proc. R. Soc. Lond. B. Biol. Sci.* **210**, 549-558.

Dabiri, J. O. (2009). Optimal vortex formation as a unifying principle in biological propulsion. *Annu. Rev. Fluid Mech.* **41**, 17-33.

Dabiri, J. O. and Gharib, M. (2005). The role of optimal vortex formation in biological fluid transport. *Proc. R. Soc. Lond. B. Biol. Sci.* **272**, 1557-1560.

Dabiri, J. O., Colin, S. P. and Costello, J. H. (2006). Fast-swimming hydromedusae exploit velar kinematics to form an optimal vortex wake. *J. Exp. Biol.* **209**, 2025-2033.

Dabiri, J. O., Colin, S. P., Katija, K. and Costello, J. H. (2010). A wake-based correlate of swimming performance and foraging behavior in seven co-occurring jellyfish species. *J. Exp. Biol.* **213**, 1217-1225.

Daniel, T. L. (1983). Mechanics and energetics of medusan jet propulsion. *Can. J. Zool.* **61**, 1406-1420.

Gharib, M., Rambod, E. and Shariff, K. (1998). A universal time scale for vortex ring formation. *J. Fluid Mech.* **360**, 121-140.

Godeaux, J. (1998). The relationships and systematics of the Thaliacea, with keys for identification. In *The Biology of Pelagic Tunicates* (ed. Q. Bone), pp. 273-294. New York: Oxford University Press.

Haddock, S. H. D. and Heine, J. N. (2005). *Scientific Blue-Water Diving*. La Jolla, CA: California Sea Grant.

Kremer, P. and Madin, L. P. (1992). Particle retention efficiency of salps. *J. Plankton Res.* **14**, 1009-1015.

Krueger, P. S. and Gharib, M. (2003). The significance of vortex ring formation to the impulse and thrust of a starting jet. *Phys. Fluids* **15**, 1271-1281.

Krueger, P. S., Dabiri, J. O. and Gharib, M. (2003). Vortex ring pinchoff in the presence of simultaneously initiated uniform background co-flow. *Phys. Fluids* **15**, L49-L52.
Krueger, P. S., Moslemi, A. A., Nichols, J. T., Bartol, I. K. and Stewart, W. J. (2008). Vortex rings in bio-inspired and biological jet propulsion. *Adv. Sci. Tech.* **58**, 237-246.
Madin, L. P. (1990). Aspects of jet propulsion in salps. *Can. J. Zool.* **68**, 765-777.
Madin, L. P. and Deibel, D. (1998). Feeding and energetics of Thaliacea. In *The Biology of Pelagic Tunicates* (ed. Q. Bone), pp. 81-103. New York: Oxford University Press.
Madin, L. P. and Purcell, J. E. (1992). Feeding, metabolism, and growth of *Cyclosalpa bakeri* in the subarctic Pacific. *Limnol. Oceanogr.* **37**, 1236-1251.
Madin, L. P., Cetta, C. M. and McAlister, V. L. (1981). Elemental and biochemical composition of salps (Tunicata: Thaliacea). *Mar. Biol.* **63**, 1432-1793.
Madin, L. P., Kremer, P., Wiebe, P. H., Purcell, J. E., Horgan, E. H. and Nemanzie, D. A. (2006). Periodic swarms of the salp *Salpa aspera* in the Slope Water off the NE United States: biovolume, vertical migration, grazing, and vertical flux. *Deep Sea Res. I.* **53**, 804-819.
Prasad, A. K. (2000). Particle image velocimetry. *Curr. Sci.* **79**, 51-60.
Raffel, M., Willert, C. E. and Kompenhans, J. (1998). *Particle Image Velocimetry: a Practical Guide*. Berlin: Springer-Verlag.
Sacrano, F. and Riethmuller, M. L. (2000). Advances in iterative multigrid PIV processing. *Exp. Fluids* **29**, S51-S61.
Stamhuis, E. J. and Videler, J. J. (1995). Quantitative flow analysis around aquatic animals using laser sheet Particle Image Velocimetry. *J. Exp. Biol.* **198**, 283-294.
Sutherland, K. R. and Madin, L. P. (2010). A comparison of filtration rates among pelagic tunicates using kinematic measurements. *Mar. Biol.* **157**, 755-764.
Vogel, S. (1994). Life in moving fluids: the physical biology of flow. Princeton, NJ: Princeton University Press.
Vogel, S. (2003). *Comparative Biomechanics.* Princeton, NJ: Princeton University Press.
Weihs, D. (1977). Periodic jet propulsion of aquatic creatures. *Fortschr. Zool.* **24**, 171-175.